Mean square optimal NUFFT approximation for efficient non-Cartesian MRI reconstruction

Zhili Yang and Mathews Jacob

Abstract

The fast evaluation of the discrete Fourier transform of an image at non-uniform sampling locations is key to efficient iterative non-Cartesian MRI reconstruction algorithms. Current non-uniform fast Fourier transform (NUFFT) approximations rely on the interpolation of oversampled uniform Fourier samples. The main challenge associated with these schemes is high memory demand due to oversampling, especially when multidimensional datasets are involved. The main focus of this work is to design an NUFFT algorithm with minimal memory demands. Specifically, we introduce an analytical expression for the expected mean square error in the NUFFT approximation based on our earlier work. We then introduce an iterative algorithm to design the interpolator and scalefactors. Experimental comparisons show that the proposed optimized NUFFT scheme provides considerably lower approximation errors than classical NUFFT schemes. The improved approximations are also seen to considerably reduce the errors and artifacts in non-Cartesian MRI reconstruction.

Keywords: interpolators, non-uniform fast Fourier transform, histogram, non-Cartesian MRI.

1. Introduction

Non-Cartesian MRI schemes (e.g., spiral and radial trajectories) offer several advantages over Cartesian sampling, including higher speed, robustness to undersampling, and low motion sensitivity. While gridding is the most popular reconstruction method [1], iterative algorithms are being increasingly used due to their improved accuracy, ability to handle image priors, and account for non-idealities during acquisition [2, 3, 4, 5]. Since the exact evaluation of the discrete time Fourier transform of the Fourier sum is computationally prohibitive, these algorithms approximate the non-Cartesian Fourier transform. While approximation schemes for specific trajectories are available [6, 7], the common approach is to compute the non-uniform samples as the interpolation of the uniform Fourier transform. The uniform Fourier samples are computed efficiently using the fast Fourier transform, while support limited functions (e.g., Kaiser–Bessel, Gaussian) are used for interpolation [8, 2, 9, 1, 10, 11]. This approximation is often termed as the non-uniform fast Fourier transform (NUFFT). NUFFT schemes often weight the signal with suitable scale factors before evaluating the uniform FFT to minimize the approximation error [12, 13, 14, 15].

Classical choices of interpolator and scale factors (e.g., Gaussian interpolator and cosine scale factors) require the Fourier transform to be evaluated on a fine uniform grid to keep the approximation error reasonably low [12, 13, 15]. The common choice is to compute the Fourier transform on a $K \times K; K = 2N$ uniform grid for an $N \times N$ image. Unfortunately, the oversampling of the Fourier

Email address: Mathews-Jacob@uiowa.edu (Zhili Yang and Mathews Jacob)
URL: http://www.engineering.uiowa.edu/~jcb/ (Zhili Yang and Mathews Jacob)

grid significantly increases the memory demands of the algorithm. For example, the reconstruction of a three dimensional dataset with $K = 2N$ requires eight times more memory than the original dataset. This often makes it difficult to accelerate such algorithms using graphical processing units (GPUs) that have limited on-board memory, especially when large datasets are involved [16]. Design strategies to optimize the interpolator by minimizing an appropriate error metric have been introduced to improve the approximation properties of the NUFFT scheme [14, 17, 18, 19, 20, 13]. All of the schemes rely on bounds for errors in the Fourier domain. The approach in the INUFFT design scheme in [21] is conceptually similar to the proposed scheme. However, the error expression is very different, mainly due to differences in key assumptions on the signal model and scale factors. In all of the current design schemes, the scale factors were assumed to be fixed [17] or have simple parametric expressions [14]. Since the constraints on the scale factors were too restrictive, the performance of the least square optimized NUFFT schemes were only comparable to the one using Kaiser-Bessel (KB) functions [14]. The NUFFT scheme was reinterpreted as a shift invariant approximation of the discrete Fourier transform (DTFT) in [22]. A worst case error metric, which was independent of the scale factors and the signal, was introduced in [22]. The optimization of this metric yielded an NUFFT scheme that provided considerably lower worst case errors than the conventional NUFFT scheme [22].

We studied the utility of the optimized interpolators [14, 22] in MR image reconstruction problems. Unfortunately, we observed that in the $K \approx N$ regime, the approximation properties of the optimized NUFFT schemes were not considerably better than that of classical methods for many images, even though the optimized NUFFT schemes yielded far lower error bounds. The main reason for this discrepancy is the use of the worst case error metrics [14, 22]. Specifically, these upper bounds for the approximation error are unrealistically high and are not achieved for practical signals. For example, the image which provides the worst case error in [22, 23] has most of its energy concentrated along the image edges/borders. Since MR brain images are often support limited to a disc region within the rectangular support, the worst case error is never achieved for such MR signals. In this context, it is desirable to derive the mean square optimal NUFFT schemes from error metrics that are more representative of real-world signals.

The main objective of this paper is to improve the framework in [22, 23] in the context of MR imaging applications and to demonstrate its utility in non-Cartesian MRI reconstruction. Specifically, we depart from the worst case setting considered in [22] and focus on a mean-square metric of the error in the NUFFT approximation. This error metric is dependent on the expected spatial energy distribution of the signal. Hence, it can be customized to real world applications (e.g., when the image is support limited to specific regions). The error metric decouples the effect of the scale factors and the interpolators into two positive terms. This enables us to derive the mean square optimal scale factors; the use of these scale factors corresponds to the projection of the DTFT of the signal to the space spanned by the integer shifts of the interpolator [22]. We adapt the iterative reweighted algorithm introduced in [22] to derive the mean square optimal interpolator and scale factors. When the spatial energy distribution of the class of signals is known *a priori* (e.g., learned from exemplar images), it will be used to derive the interpolator. Empirically, we observe that the NUFFT scheme that is derived with the assumption of uniform energy distribution is comparable to the one using known energy distribution for many practical signals; the assumption of uniform energy distribution is a better alternative than using the worst case scenario when the energy distribution is unknown.

We validate the proposed mean square optimal NUFFT scheme using simulations and experimental MRI data. Our experiments show that the proposed scheme is capable of providing good

approximations of the non-uniform DTFT for modest oversampling factors ($K < 1.1 \times N$) and short interpolators ($J \leq 6$). The image reconstruction experiments show that the proposed scheme provides more accurate reconstructions than classical NUFFT schemes, when low oversampling factors are considered. The low oversampling factor will in turn translate to memory efficient algorithms which will enable its implementation on faster devices such as GPUs that have limited onboard memory. While the reduction in memory demand may come in with a slight increase in computational complexity compared to $K = 2N$, the speedups offered by faster parallel computing devices are expected to more than make up for the performance.

2. Methods

2.1. NUFFT approximation: Background

The NUFFT scheme approximates the discrete Fourier transform (DTFT) of the uniform support limited signal $x[n]$; $n = -N/2, ..., N/2 - 1$:

$$\hat{x}(\nu) = \sum_{n=-N/2}^{N/2-1} x[n]\, e^{-\frac{j2\pi n\nu}{N}} \tag{1}$$

at non-uniform k-space locations ν_m; $m = 0, ..., M-1$. The exact evaluation of the discrete time Fourier transform of this sum is computationally expensive. In their seminal work [12], Dutt and Rokhlin have shown that an exponential with arbitrary frequency ν can be efficiently approximated as:

$$e^{-\frac{j2\pi n\nu}{N}} \approx \underbrace{\exp\left(b\,|n|^2\right)}_{h[n]} \sum_{k=\nu/T-J/2}^{k=\nu/T+J/2} \varphi\left(\frac{\nu}{T} - k\right) e^{-\frac{j2\pi kT}{N}}. \tag{2}$$

Here, φ is the Gaussian interpolation function and $T = N/K < 1$, where K is an appropriately chosen integer. In [24], the authors extended the above approximation using alternate interpolation functions and associated weighting functions . The NUFFT scheme is obtained by substituting the approximation specified by (2) into (1). Thus, the NUFFT approximation involves two key steps. The K-point FFT ($K > N$) of the sequence $h[n]x[n]$ is first computed as

$$c[k] = \sum_{n=-N/2}^{N/2-1} h[n]x[n]\, e^{-\frac{j2\pi kn}{K}}, \tag{3}$$

where $h[n]; n = -N/2, ..., N/2 - 1$ are scale factors[1]. Once the coefficients $c[k]$ are available, the NUFFT approximation of the DTFT is obtained as:

$$\hat{x}_{\text{app}}(\nu) = \sum_{k=-K/2}^{K/2-1} c[k]\, \varphi_p\left(\frac{\nu}{T} - kT\right), \tag{4}$$

where $T = N/K$ is the sampling step and $\varphi_p(x) = \sum_{k\in\mathbb{Z}} \varphi(x - kN)$ is the K-periodized version of φ.

[1] In the Gaussian case, the scale factors are specified by $\exp(b\,|n|^2)$.

2.2. Current NUFFT design strategies

The error in the NUFFT approximation of a signal $x[n]$ at a specific frequency point ν is specified by

$$\underbrace{\hat{x}(\nu) - \hat{x}_{\text{app}}(\nu)}_{\epsilon(\nu)} = \left\langle x[n], \underbrace{e^{-\frac{j2\pi n\nu}{N}} - h[n] \sum_{k=-K/2}^{K/2-1} \varphi\left(\frac{\nu}{T} - k\right) e^{-\frac{j2\pi nk}{K}}}_{q_\nu[n]} \right\rangle \tag{5}$$

Several researchers have derived the upper-bound of the approximation error based on this expression [15, 20, 14]:

$$\|\epsilon(\nu)\| \quad \leq \quad \|\mathbf{x}\|_{\ell_2} \cdot \ \|\mathbf{q}_\nu\|_{\ell_2} \tag{6}$$

For example, the Nguyen *et al.,* and Nieslony *et al.,* proposed to determine the interpolator φ by minimizing $\|\mathbf{q}_\nu\|_{\ell_2}$, assuming pre-selected scale factors (e.g., Gaussian, Kaiser-Bessel, Cosine) [15, 20]. Since this is a quadratic optimization problem, the optimal interpolator is solved analytically. However, the assumption of fixed scale factors makes it difficult for the scheme to exploit the full flexibility to lower the approximation error. This approach is similar to [14], where they additionally used a min-max scheme to also search for the scale factors. However, since their search was restricted to small parametric families, this approach could not exploit the full potential of the NUFFT approximation.

All of the above NUFFT design schemes evaluated the point-wise error in the Fourier domain $\epsilon(\nu)$. Duijndam *et al.,* focussed on numerically optimizing the INUFFT approximation scheme in [21]. They assume the signal in the Fourier domain to be modeled as a linear combination of Diracs at the non-uniform sampling locations:

$$\hat{x}(\nu) = \sum_i d_i \ \delta(\nu - \nu_i),$$

and derive the expression for the error in the spatial domain as

$$\|x[n] - x_{\text{INUFFT}}[n]\|^2 = \|x[n]\|^2 \ D\left(\frac{2\pi n}{K}\right). \tag{7}$$

Here,

$$D(\nu) = \sum_{l\neq 0} \frac{|\hat{\varphi}(\nu + lK)|^2}{|\hat{\varphi}(\nu)|^2}. \tag{8}$$

Here, they assumed the scale factors to be chosen as $h[n] = 1/\hat{\varphi}(2\pi n/K)$. They proposed a numerical algorithm to determine the mean square optimal INUFFT interpolator that minimizes the mean square error $\sum_n \|x[n] - x_{\text{INUFFT}}[n]\|^2$. Although this INUFFT design scheme has conceptual similarities with the proposed schemes, it cannot be directly applied to our NUFFT setting. Besides, their error expression is very different from the proposed scheme since they assume a specific signal model and scale factors.

2.3. Mean square error metric in NUFFT approximation

We have shown that the NUFFT scheme is the shift invariant approximation of $\hat{x}(\nu)$ in the periodic shift invariant space V_{φ_p}, spanned by the function φ [22]. Specfically, the coefficients can

be seen as the inner-products between the exact DTFT of $x[n]$ and shifted versions of the analysis function:

$$c[k] = \left\langle \hat{x}(\nu), \tilde{\varphi}_p^* \left(\frac{\nu}{T} - k \right) \right\rangle_{L_2[-\pi,\pi]}.$$

The analysis function is the DTFT of the scale factors $\tilde{\varphi}_p(\nu) = \sum_{n=-N/2}^{N/2-1} h[n] e^{-j\frac{2\pi\nu}{K}}$. The re-interpretation of the NUFFT scheme as a shift invariant representation enables us to use the theoretical tools developed for periodic shift invariant representations to analyze and optimize the NUFFT scheme.

We have derived an expression for the error in the NUFFT approximation as [25, 22]:

$$\eta\left(x, \varphi, \tilde{\varphi}, K\right) \quad = \quad \sum_{n=-N/2}^{N/2-1} |x[n]|^2 \, E_{\varphi,\tilde{\varphi}}\left(\frac{2\pi n}{K}\right), \tag{9}$$

where the error kernel $E_{\varphi,\tilde{\varphi}}(\omega)$ is given by

$$E_{\varphi,\tilde{\varphi}}\left(-\omega\right) = \underbrace{1 - \frac{\left|\hat{\varphi}(\omega)\right|^2}{\hat{a}_\varphi(\omega)}}_{E_{\min,\varphi}} + \underbrace{\hat{a}_\varphi(\omega) \left| \hat{\tilde{\varphi}}(\omega) - \hat{\varphi}_d(\omega) \right|^2}_{E_{\mathrm{res},\varphi,\tilde{\varphi}}}. \tag{10}$$

Here, $\hat{\varphi}(\omega) = \int_{-\infty}^{\infty} \varphi(\nu) e^{-j\nu\omega} d\nu$ is the Fourier transform of the interpolator $\varphi(\nu)$ and $\hat{a}_\varphi(\omega) = \sum_{k\in\mathbb{Z}} \left|\hat{\varphi}(\omega + 2k\pi)\right|^2$ is the discrete Fourier transform of the autocorrelation sequence of the interpolator $a_\varphi(k) = \langle \varphi(\nu), \varphi(\nu - k) \rangle$. The dual function of the interpolator, denoted by φ_d in (10) is specified by

$$\hat{\varphi}_d(\omega) = \hat{\varphi}(\omega) / \hat{a}_\varphi(\omega). \tag{11}$$

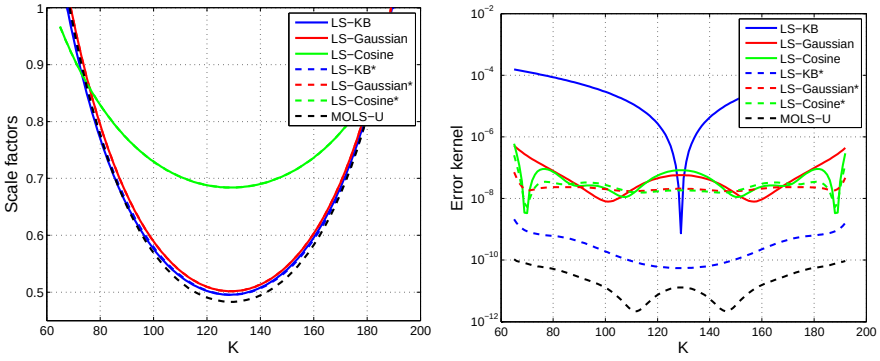

(a) scale factors (b) Error kernels

Figure 1: Effect of scale factors on NUFFT approximation: the solid lines correspond to least square methods introduced in [20, 15, 14] with KB, Gaussian, and cosine scale factors. Note that all of these methods results in considerably higher error kernels than the proposed MOLS-U interpolator, shown in black dotted lines. To demonstrate the improvement offered by mean-square optimal scale factors specified by (13), we re-compute the scale factors of the LS schemes [20, 15, 14]; the corresponding methods are termed as LS-KB*, LS-Cosine*, and LS-Gaussian*, which are denoted by dotted lines. We observe that the error kernels of these methods are considerably lower and more comparable to the proposed scheme than the original LS methods. These results demonstrate the benefit in co-designing the interpolator and the scale factors.

2.4. Selection of scale factors

Note that $E_{\min,\varphi}(\omega)$ and $E_{\text{res},\varphi,\tilde{\varphi}}$ are positive functions of ω. The first term

$$E_{\min,\varphi}(\omega) = \frac{\sum_{k\neq 0} |\hat{\varphi}(\omega + 2k\pi)|^2}{\sum_{k\in\mathbb{Z}} |\hat{\varphi}(\omega + 2k\pi)|^2} \tag{12}$$

is independent of the analysis function $\tilde{\varphi}$. This term quantifies the error in orthogonally projecting the DTFT of the signal to the subspace spanned by the shifts of the interpolator $\{\varphi\left(\frac{\nu}{T} - k\right), k = -K/2, .., K/2\}$. Note that when $|\varphi(\omega + 2k\pi)| << |\varphi(\omega)|, \forall k \neq 0$, we have $E_{\min,\varphi}(\omega) \to 0$. This may partially explain the relatively good performance of support limited functions, whose energy is concentrated in a certain frequency range (e.g., Kaiser-Bessel, prolate spheroidal functions) [18, 13, 24].

The second term $E_{\text{res},\varphi,\tilde{\varphi}}$ will vanish if $\tilde{\varphi}_d(\omega) = \varphi_d(\omega)$. This choice corresponds to the mean square optimal scale factors

$$h_d[n] = \frac{\hat{\varphi}(2\pi n/K)}{\sum_{k\in\mathbb{Z}} |\hat{\varphi}(2\pi n/K + 2k\pi)|^2}. \tag{13}$$

We observe that the classical choice of scale factors $h[n] = 1/\hat{\varphi}(2\pi n/K)$ will result in a higher error than with the mean square optimal scale factors. Specifically, we have

$$E_{\text{res},\varphi,\tilde{\varphi}} = \hat{a}_\varphi(\omega) \left| \frac{1}{\hat{\varphi}(\omega)} - \frac{\hat{\varphi}(\omega)}{\hat{a}_\varphi(\omega)} \right|^2 = \frac{1}{\hat{a}_\varphi(\omega)} \left(\sum_{k\neq 0} \frac{|\hat{\varphi}(\omega + 2k\pi)|^2}{|\hat{\varphi}(\omega)|^2} \right)^2. \tag{14}$$

Note that this term is also dependent on the ratio $\sum_{k\neq 0} |\varphi(\omega + 2k\pi)|^2 / |\varphi(\omega)|^2$. This implies that the residual error will be smaller for interpolators that [13, 18].

2.5. Optimization of the interpolator

A careful optimization of these factors is essential to minimize the approximation error, while keeping resources such as memory and computational complexity to a minimum. If the scale factors are chosen as in (13), the NUFFT approximation is the orthogonal projection of the exact DTFT (1) of the signal to the shift invariant subspace spanned by $\{\varphi(\frac{\nu}{T} - k), k \in \mathbb{Z}\}$. This minimum achievable error is specified by

$$\eta_{\min}(x, \varphi, K) = \sum_{n=-N/2}^{N/2-1} |x[n]|^2 E_{\min,\varphi}\left(\frac{2\pi n}{K}\right). \tag{15}$$

$$\varphi_{\text{wols}} = \arg\min_{\varphi} \sum_{n=-N/2}^{N/2-1} \left| E_{\min,\varphi}\left(\frac{2\pi n}{K}\right) \right|^2 \quad \text{such that} \quad \sum_{n\in\mathbb{Z}} \left| \hat{\varphi}\left(\frac{2\pi n}{K}\right) \right|^2 = 1. \tag{16}$$

Note that this expression is only dependent on the interpolator φ, the signal $x[n]$, and the sampling step $T = N/K$. Evaluating the expectation on both sides of the above expression, we obtain

$$e(\varphi, K) = \mathbb{E}\ (\eta_{\min}) = \sum_{n=-N/2}^{N/2-1} s[n]\, E_{\min,\varphi}\left(\frac{2\pi n}{K}\right), \tag{17}$$

where $s[n] = \mathbb{E}\ \left(|x[n]|^2\right)$ is the energy distribution of the class of the signals. Note that if $s[n] = 1, \forall n$, then $e(\varphi, K) = \sum_{n=-N/2}^{N/2-1} E_{\min,\varphi}\left(\frac{2\pi n}{K}\right)$.

2.6. Mean square optimal NUFFT interpolator

We derive the mean square optimal NUFFT interpolator as the one that minimizes the expected error specified by (17) subject to the energy constraint $\|\varphi\|_{L_2} = 1$:

$$\varphi_{\text{opt}} = \arg\min_{\varphi} e(\varphi, K) \;\; \text{such that} \;\; \sum_{n\in\mathbb{Z}} \left|\hat{\varphi}\left(\frac{2\pi n}{K}\right)\right|^2 = 1. \tag{18}$$

Substituting for the expression of $E_{\min,\varphi}$ from (10) and using the relation $\hat{a}_{\varphi}(\omega) = \sum_{k\in\mathbb{Z}} |\hat{\varphi}(\omega + 2k\pi)|^2$, we obtain:

$$e(\varphi, K) = S - \sum_{n=-N/2}^{N/2-1} s[n] \left(\frac{|\hat{\varphi}(-2\pi n/K)|^2}{\sum_{k\in\mathbb{Z}} |\hat{\varphi}(-2\pi n/K + 2k\pi)|^2}\right), \tag{19}$$

where the constant $S = \sum_{n=-N/2}^{N/2-1} s[n]$ is the total energy of the signal. Omitting S, the optimization simplifies to the minimization of the second part of (19). Note that the above criterion is a non-quadratic expression of the Fourier coefficients of the interpolator. Since the direct minimization of this expression is difficult, we propose to adapt the iterative reweighted minimization algorithm introduced in [22] to determine the mean square optimal interpolator. Using (19), we rewrite (18) as

$$\begin{aligned} \varphi_{\text{opt}} \;\; = \;\; \arg\max_{\varphi} & \sum_{n=-\frac{N}{2}}^{\frac{N}{2}-1} w[n] \left|\hat{\varphi}\left(-\frac{2\pi n}{K}\right)\right|^2 \\ & \text{such that} \;\; \sum_{n\in\mathbb{Z}} \left|\hat{\varphi}\left(\frac{2\pi n}{K}\right)\right|^2 = 1. \end{aligned} \tag{20}$$

Here, the weights $w[n]$ are specified by

$$w[n] = \frac{s[n]}{\sum_{k\in\mathbf{Z}} |\hat{\varphi}\left(-2\pi n/K + 2k\pi\right)|^2}. \tag{21}$$

We use an iterative scheme that alternates between (20) and (21). At each iteration, the algorithm assumes the weights $w[n]$ to be constants and solves (20) to determine the interpolator. Once interpolator is obtained by solving (20), the weights $w[n]$ are re-estimated. The steps (20) and (21) are repeated in an alternating fashion until the cost function does not change considerably[2]. We initialize the algorithm by setting the weights as $w[n] = s[n]$.

2.7. Discretization of the interpolator

The NUFFT approximation of the signal (4) at a specified non-uniform location $\nu \in \mathbb{R}$ requires the evaluation of the samples of the interpolator $\varphi(\nu - m); m \in \mathbb{Z}$. The exact evaluation of the discrete time Fourier transform of the samples at several non-Cartesian locations is computationally

[2]We currently do not have guarantees for the convergence of this algorithm to the global minimum of the cost function. Nevertheless, the interpolator and prefilter obtained by the proposed algorithm are observed to considerably reduce the approximation error over classical schemes.

prohibitive in MR image reconstruction algorithms, even when the interpolator has analytical expressions (e.g., Gaussian or Kaiser-Bessel interpolators). Hence, it is a general practice to pre-compute the interpolator on a fine uniform grid and store it as a lookup table; the samples of the interpolators are then obtained as a linear interpolation of these uniformly sampled values. Note that the performance loss in discretizing the interpolator could be ignored if the grid is densely sampled. The evaluation for each interpolator sample requires two multiplications and one addition; the computational complexity is independent of the grid density. Assuming an even interpolator oversampling factor O, we assume the interpolator φ to be represented as:

$$\varphi(\nu) = \sum_{k=-JO/2+1}^{JO/2-1} q[k]\beta(O\nu - k) \tag{22}$$

Here, $q[k] = \varphi(\frac{k}{O}), k = -JO/2+1, ..JO/2-1$ are the uniform samples of the interpolator and β denotes the linear B-spline function. The Fourier transform of the interpolator is given by $\hat{\varphi}(\omega) = \hat{q}(e^{j\frac{\omega}{O}})\hat{\beta}(\frac{\omega}{O})$. Substituting the expression of $\hat{\varphi}(\omega)$ back in (20), we obtain

$$\begin{aligned} \mathbf{q}_{\text{opt}} &= \arg\max_{\mathbf{q}} \sum_{n=-\frac{N}{2}+1}^{\frac{N}{2}} u[n] \left|\hat{q}\left(e^{-\frac{2\pi n}{K}}\right)\right|^2 \\ &\qquad \text{such that} \sum_{n=-RN}^{RN} b[n] \left|\hat{q}\left(e^{-\frac{2\pi n}{K}}\right)\right|^2 = 1. \end{aligned} \tag{23}$$

Here, the weights are specified by

$$u[n] = w[-n]\left|\hat{\beta}\left(\frac{2\pi n}{KO}\right)\right|^2, \quad \text{and} \tag{24}$$

$$b[n] = \left|\hat{\beta}\left(\frac{2\pi n}{KO}\right)\right|^2. \tag{25}$$

Note that the second summation is now restricted to a finite range $[-RN, RN]$, where R is a sufficiently large number (we chose it as 20 in this study[3]).

Since the interpolator is support limited, the DTFT of the sequence $q[k]; n = -JO/2+1, ..JO/2-1$ simplifies to a finite summation. Hence, $\hat{\mathbf{q}} = \mathbf{F}\mathbf{q}$, where $\hat{\mathbf{q}}$ is the vector of Fourier samples, $\mathbf{q}$ is the vector of coefficients, and $\mathbf{F}$ is the $(2RN) \times (JO-1)$ discrete Fourier transform matrix. Thus, the optimization problem specified by (20) can be reformulated in the matrix form as

$$\mathbf{q}_{\text{opt}} = \arg\max_{\mathbf{q}} \ \mathbf{q}^T \left(\mathbf{F}^T \, \mathbf{U} \, \mathbf{F}\right) \mathbf{q} \quad \text{subject to} \quad \mathbf{q}^T \ \mathbf{B} \ \mathbf{q} = 1 \tag{26}$$

Here, $\mathbf{U} = \text{diag}(u[n])$ and $\mathbf{B} = \text{diag}(b[n])$. Note that (26) is the generalized eigenvalue problem [26]; the solution is obtained as the eigenvector corresponding to the maximum eigenvalue of the pair of matrices $(\mathbf{F}^T\mathbf{U}\mathbf{F}, \mathbf{B})$. The iterative reweighted algorithm proceeds by alternating between the generalized eigenvalue problem (26) and re-evaluation of the weights $w[n]$, and hence the diagonal

[3]We studied the dependence of the approximation on R and determined that $R = 20$ results in minimal truncation error.

matrix $\mathbf{U}$, until convergence. The pseudo-code of the algorithm is shown below. The implementation of the NUFFT algorithm as well as sample codes for MRI reconstruction from non-Cartesian samples are available for download at https://research.engineering.uiowa.edu/cbig/content/software.

Algorithm : MOLS NUFFT$(s[n], K, N, J, \text{Ofactor})$

$\varphi \leftarrow$ Kaiser Bessel function
$\text{err} = 1 \times 10^{10}$
while $|\text{err} - e(\varphi, K)| < \text{THRESHOLD} \times e(\varphi, K)$
do
- $\text{err} \leftarrow e(\varphi, K)$, specified by (17)
- Update $w[n]$ using (21)
- $\mathbf{U} \leftarrow \text{diag}(u[n])$, where $u[n]$ is specified by (24)
- $\mathbf{B} \leftarrow \text{diag}(b[n])$, where $b[n]$ is specified by (25)
- Compute $\mathbf{q}_{\text{opt}}$ using (26)

Compute $\mathbf{h}_{\text{opt}}$ using (13)
return $(\mathbf{q}, \mathbf{h}_{\text{opt}})$

2.8. Experiments

We assess the utility of the proposed NUFFT approximation algorithms in recovering images from their non-Cartesian Fourier samples. We consider numerical simulations in Fig. 3 and Fig. 4, where the non-Cartesian Fourier samples were generated using the exact discrete Fourier transform on radial trajectories. The image $f(\mathbf{r})$ is recovered from the non-Cartesian samples specified by the vector $\mathbf{b}$ using the total variation (TV) regularized reconstruction scheme:

$$f_{\text{recon}} = \arg \min_{f} \|\mathcal{A}(f) - \mathbf{b}\|^2 + \lambda \|\nabla f\|_{\ell_1}. \tag{27}$$

Here, $\mathcal{A}$ is discrete Fourier transform of the image f computed at the non-Cartesian sampling locations. We solve the optimization problem (27) by adapting the alternating minimization algorithm, described in detail in [27]. The main modification involved changing the forward model $\mathcal{A}$ and its adjoint $\mathcal{A}^{\mathcal{T}}$. Since the exact Fourier replacement step used in [27] cannot be used in our setting, we solved this sub-problem using conjugate gradients algorithm.

We study the impact of different NUFFT approximations of $\mathcal{A}$ operator on the quality of the reconstructions. Specifically, we compare the proposed mean square optimal least square (MOLS) interpolator which assumes uniform energy distribution (MOLS-U), worst case mean square optimalleast square (WOLS) interpolator [22], and the least square interpolator proposed in [20] based on Kaiser-Bessel scale factors (LS-KB). We rely on the discretization of the interpolators, specified by (22), to compute the mean square optimal scale factors. Note that these scale factors provide improved approximations over scale factors used in classical NUFFT schemes.

The brain dataset in Fig. 3 corresponds to an acquisition using 12 channel head coil using a variable density multi-shot spiral acquisition using a with the following specifications: # interleaves=24, FOV=20 cm, 192×192 matrix, resulting in an in-plane spatial resolution of 1.04×1.04 mm^2. The data from each of the channels are independently recovered using (27), before combining them using the sum of squares approach.

3. Results

The proposed optimization scheme is designed to minimize the error in approximating the exact DTFT of support limited images. We first determine the utility of the interpolators in obtaining a good approximation of the discrete Fourier transform. We then study the impact of the NUFFT approximation quality on recovering MR images from its non-Cartesian k-space samples is then determined using both numerical simulations and experimental data. The proposed mean square optimal (MOLS) interpolators are compared against the interpolators optimized using the worst case interpolation error metric (termed as WOLS interpolators) as well as blue the least square interpolators using Kaiser-Bessel scale factors (LS-KB).

3.1. Analysis of NUFFT approximation error

We study the utility of co-designing the interpolators and scalefctors in Fig. 1. Specifically, we compare the NUFFT schemes in [20, 15, 14] with KB, Gaussian, and cosine scale factors, against the proposed mean square optimal NUFFT scheme assuming a uniform error distribution (MOLS-U). We observe that the conventional schemes result in considerably higher error kernels than the MOLS-U method. We observe that the errors provided by the classical schemes can be considerably reduced if their scale factors are recomputed according to (13); they are more comparable to the MOLS scheme than the original LS NUFFT schemes [20, 15, 14]. These results demonstrate the benefit in co-designing the interpolator and the scale factors.

We illustrate the ability of the NUFFT interpolators to reduce approximation errors for signals with a known energy distribution in Fig. 2. Specifically, we assume the spatial energy distribution $s[n]$ to be a truncated Gaussian function, shown in Fig.2(j). We set $K = 68$ and $N = 64$ ($K/N = 1.0625$), while the interpolators were discretized on a grid assuming $O = 101$. The optimal interpolators and scale factors corresponding to worst case error metric (WOLS) [22], the proposed mean square error metric (MOLS), the MOLS scheme assuming a uniform error distribution (MOLS-U), and the least square interpolator with KB scale factors (LS-KB) computed according to [20, 15, 14] are shown in Fig.2.(a)-(f). The error kernels $E_{\min,\varphi}(\frac{2\pi n}{K})$ corresponding to WOLS,LS-KB,MOLS and MOLS-U are shown in Fig.2.(g)-(i), respectively. We observe that the worst case interpolator results in flatter error kernels, which lead to roughly the same level of errors in all image regions. This is expected since it is minimizing the worst case error. In contrast, the MOLS interpolators provide lower value of error kernels in the central regions corresponding to the peak of $s[n]$ at the expense of slightly higher errors close to the image boundaries. Since $s[n]$ has smaller values at the boundaries, the MOLS interpolators will result in lower expected error. While the LS-KB interpolator generally have lower errors in the central regions, we observe that the errors with this method is considerably higher than the proposed schemes. The poor performance of LS-KB scheme can be mainly attributed to the sub-optimal scale factors.The plot of the mean square and worst case errors as a function of the size of the interpolator is shown in (k) and (l), respectively. We observe from (l) that the WOLS interpolators provide considerably lower worst case errors at higher values of J. However, the mean-square performance of these interpolators are worse than the MOLS interpolators as seen from (k). We also observe that the performance of MOLS-U interpolator is not considerably worse than the MOLS scheme; this approximation can be used when the exact energy distribution is unknown.

3.2. Utility of the proposed NUFFT in MRI reconstruction

We first consider the reconstruction of the 128x128 MRI knee image from its samples on 128 uniformly spaced radial lines in Figure 3. Since the image has high energy close to the top and

bottom edges, it is challenging to approximate the DTFT of this image using classical NUFFT schemes. We set $K = 130; J = 6$ and recover the images using different NUFFT approximations. Note that the oversampling factor is $\frac{K}{N} = 1.016$. The reconstructions with $K = 130$ are compared against the images recovered using classical $K = 2N; J = 6$ LS-KB NUFFT. We observe that in the K=130 setting, the LS-KB NUFFT [20] scheme results in reconstructions with considerable line-like artifacts (see (b) and (f), as well as the zoomed images (j) and (n)). The worst case (WOLS) scheme is able to significantly lower the streak-like artifacts, but still suffers from artifacts in the top and middle regions (see from zoomed images of the top of the image in (k) and the middle section in (o)). By contrast, the mean-square NUFFT scheme (MOLS-U) is capable of reducing the overall error without significantly increasing artifacts. Note that the reconstruction is mostly free of artifacts, except for some minor streaks at the top right corner (see zoomed image in (l).

The knee reconstructions with $K = 132$ are shown in Fig. 4. We observe that the LS-KB scheme still suffers from artifacts, which are visible from the zoomed images in (j) and (n). The proposed WOLS scheme is considerably better, but still has relatively minor residual artifacts. The MOLS scheme is seen to provide results that are quite comparable to the K=256 KB scheme (see Fig. 3.(a) as well as Fig. 4.(e), (i) and (m). Specifically, the use of the slightly larger K value removed the streaks in the top right corner, which was seen in the K=130 case (Fig. 3.l). These experiments demonstrate the benefit of the proposed scheme in providing good quality reconstructions for low values of K, while providing results that are close to the K=2N setting.

We determine the use of the proposed NUFFT approximation in the recovery of the brain image from its spiral samples in Fig. 5. We set $K = 194$ and $J = 4$, while the size of image N is 192; $\frac{K}{N} = 1.01$. The TV reconstructed images with different NUFFT approximations are compared against the one using the classical LS-KB scheme with $K = 2N$ in Fig. 3. We observe that the MOLS-U scheme is capable of providing reconstructions that closely match the classical choice corresponding to K=2N setting. The WOLS scheme is observed to introduce oscillatory textures in the reconstruction, which can be better appreciated from the zoom of the original images. The LS-KB scheme with $K = 194$ introduces considerably larger errors. These experiments confirm that the use of the proposed interpolators can provide substantially lower error than classical interpolators. Thus, the proposed algorithms can achieve relatively high accuracy with considerably lower memory demands than classical schemes.

4. Discussion and Conclusion

We introduce a design strategy to determine the mean square optimal interpolator and scale factors in the NUFFT approximation. Our main goal is to improve the quality of the NUFFT approximation, which is especially relevant in the context of low oversampling factors ($K/N \approx 1$) which are needed for the implementation of MRI reconstruction algorithms on devices with limited onboard memory. We determine the mean square optimal NUFFT scheme by minimizing a novel analytical expression for the expected mean square error in a NUFFT approximation. We observe that the proposed error expression is more representative of real-world signals compared to the worst case one in [22]. Our experiments demonstrate that we can obtain good non-Cartesian MRI images by using the mean square optimal interpolators and scale factors, even when $\frac{K}{N} < 1.1$ and $J \leq 6$. Thus, the proposed scheme enables us to considerably reduce the memory demand for non-Cartesian reconstructions, which makes it possible to accelerate these algorithms using graphical processing units.

5. Acknowledgements

We thank the insightful comments by the anonymous reviewers that considerably improved the quality of the paper. This work is supported by grants NSF CCF-0844812, NSF CCF-1116067, NIH 1R21HL109710-01A1, ONR-N000141310202, and ACS RSG-11-267-01-CCE.

References

[1] P. Beatty, D. Nishimura, J. Pauly, Rapid gridding reconstruction with a minimal oversampling ratio, IEEE Transactions on Medical Imaging 24 (6) (2005) 799–808.

[2] B. Sutton, D. Noll, J. Fessler, Fast, iterative image reconstruction for MRI in the presence of field inhomogeneities, IEEE Transactions on Medical Imaging, 22 (2) (2003) 178 – 188.

[3] J. Fessler, Model-based image reconstruction for MRI, IEEE Signal Processing Magazine 27 (4) (2010) 81–89.

[4] R. Eslami, M. Jacob, Robust reconstruction of MRSI data using a sparse spectral model and high resolution MRI priors, IEEE Transactions on Medical Imaging 29 (6) (2010) 1297–1309.

[5] S. Bhave, R. Eslami, M. Jacob, Sparse spectral deconvolution algorithm for non-Cartesian MR spectroscopic imaging, Magnetic Resonance in Medicine (1522-2594).

[6] C. K. Turnes, J. Romberg, Efficient Calculations of 3-D FFTs on spiral contours, Journal of Scientific Computing 50 (3) (2012) 610–628.

[7] C. K. Turnes, J. Romberg, Spiral FFT: an efficient method for 3-D FFTs on spiral MRI contours, in: 17th IEEE International Conference on Image Processing (ICIP), 2010, IEEE, 2010, pp. 617–620.

[8] K. Pruessmann, M. Weiger, P. Börnert, P. Boesiger, Advances in sensitivity encoding with arbitrary k-space trajectories, Magnetic Resonance in Medicine 46 (4) (2001) 638–51.

[9] H. Eggers, T. Knopp, D. Potts, Field inhomogeneity correction based on gridding reconstruction for magnetic resonance imaging, IEEE Transactions on Medical Imaging 26 (3) (2007) 374 – 384.

[10] J. Jackson, C. Meyer, D. Nishimura, A. Macovski, Selection of a convolution function for Fourier inversion using gridding, IEEE Transactions on Medical Imaging 10 (3) (1991) 473–478.

[11] G. E. Sarty, R. Bennett, R. W. Cox, Direct reconstruction of non-Cartesian k-space data using a nonuniform fast Fourier transform, Magnetic Resonance in Medicine 45 (5) (2001) 908–915.

[12] A. Dutt, V. Rokhlin, Fast Fourier transforms for nonequispaced data, SIAM J. Sci. Comput. 14 (6) (1993) 1368–1393.

[13] D. Potts, G. Steidl, M. Tasche, Fast Fourier transforms for nonequispaced data: A tutorial, Modern Sampling Theory: Mathematics and Applications (2001) 247–270.

[14] J. Fessler, B. Sutton, Nonuniform fast Fourier transforms using min-max interpolation, IEEE Transactions on Signal Processing 51 (2) (2003) 560–574.

[15] N. Nguyen, Q. Liu, The regular Fourier matrices and nonuniform fast Fourier transforms, SIAM J. Sci. Comput. 21 (1) (1999) 283–293.

[16] M. Murphy, M. Zarrouk, K. Keuter, M. Lustig, nuFFTW: A parallel auto-tuning library for performance optimization of the nuFFT, in: Proceedings of the 21th Annual Meeting of the ISMRM, 2013.

[17] L. Sha, H. Guo, A. Song, An improved gridding method for spiral MRI using nonuniform fast Fourier transform, Journal of Magnetic Resonance 162 (2) (2003) 250–258.

[18] J. Fessler, On NUFFT-based gridding for non-Cartesian MRI, Journal of Magnetic Resonance 188 (2) (2007) 191–195.

[19] G. Steidl, A note on fast Fourier transforms for nonequispaced grids, Adv. Comput. Math. 9 (3-4) (1998) 337–352.

[20] A. Nieslony, G. Steidl, Approximate factorizations of Fourier matrices with nonequispaced knots, Linear Algebra and its Applications 366 (2003) 337–351.

[21] A. Duijndam, M. Schonewille, Nonuniform fast Fourier transform, Geophysics 64 (2) (1999) 539–551.

[22] M. Jacob, Optimized least-square nonuniform fast Fourier transform, IEEE Transactions on Signal Processing 57 (6) (2009) 2165–2177.

[23] Z. Yang, M. Jacob, Efficient NUFFT algorithm for non-Cartesian MRI reconstruction, in: IEEE International Symposium on Biomedical Imaging: From Nano to Macro, 2009. ISBI'09., IEEE, 2009, pp. 117–120.

[24] N. Nguyen, Q. Liu, The regular Fourier matrices and nonuniform fast Fourier transforms, SIAM Journal on Scientific Computing 21 (1) (1999) 283–293.

[25] M. Jacob, T. Blu, M. Unser, Sampling of periodic signals: A quantitative error analysis, IEEE Transactions on Signal Processing, 50 (5) (2002) 1153–1159.

[26] G. H. Golub, C. F. Van Loan, Matrix computations. 1996, Johns Hopkins University, Press, Baltimore, MD, USA.

[27] Y. Wang, J. Yang, W. Yin, Y. Zhang, A new alternating minimization algorithm for total variation image reconstruction, SIAM Journal on Imaging Sciences 1 (3) (2008) 248–272.

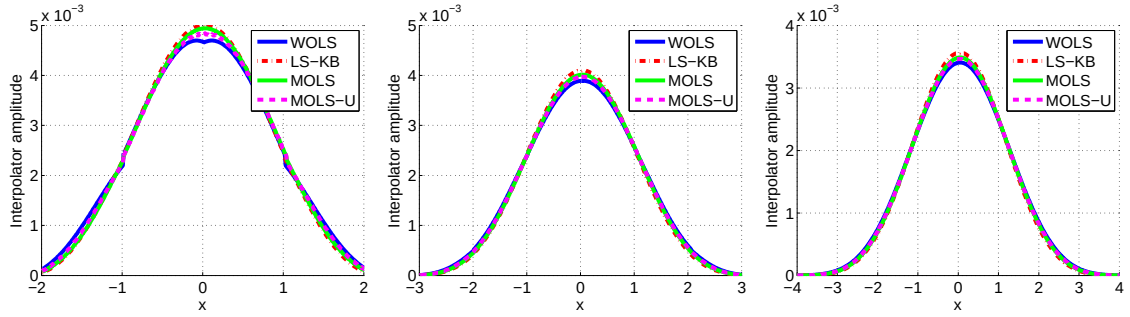

(a) Interpolators,J=4 (b) Interpolators,J=6 (c) Interpolators,J=8

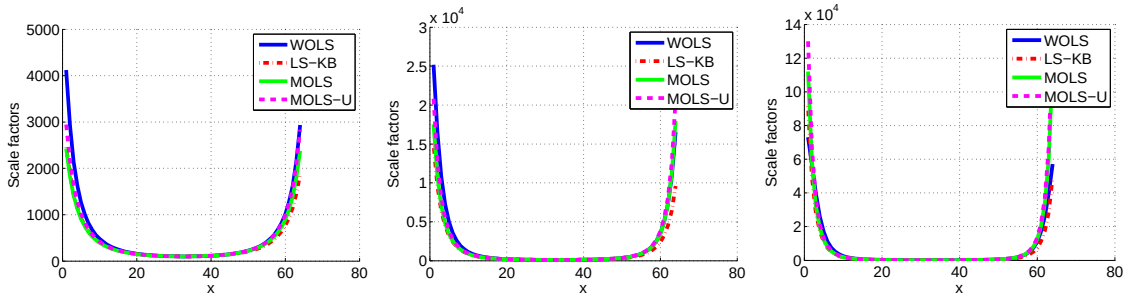

(d) Prefilters,J=4 (e) Prefilters,J=6 (f) Prefilters,J=8

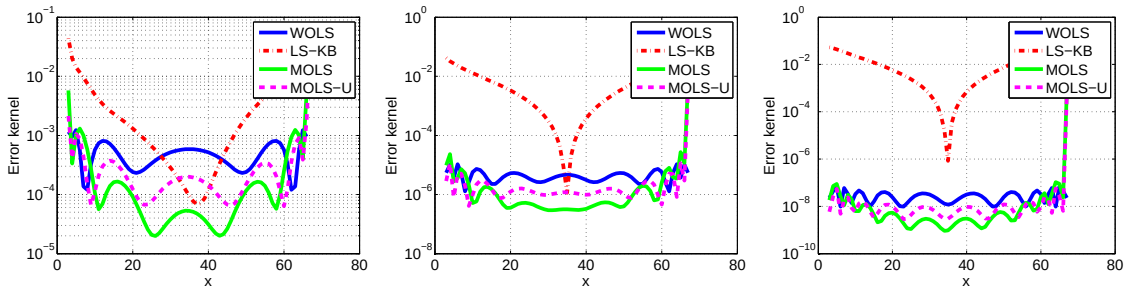

(g) Error kernels,J=4 (h) Error kernels,J=6 (i) Error kernels,J=8

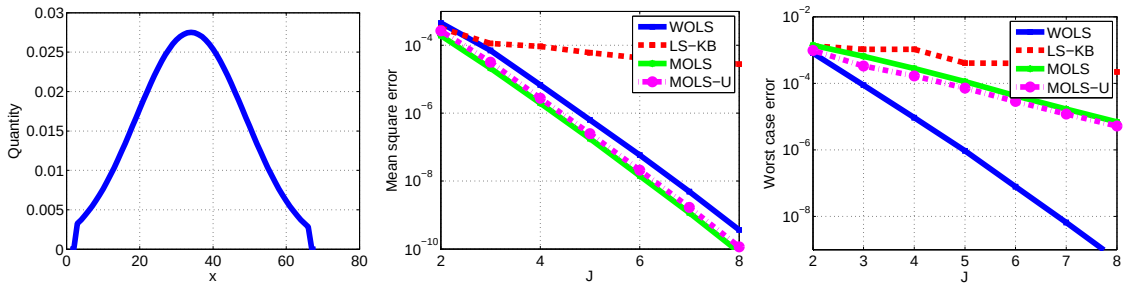

(j) Energy distribution: $s(n)$ (k) Mean square error vs J (l) Worst case error vs J

Figure 2: Comparison of different NUFFT approximation schemes:the optimized interpolators, scale factors, and the corresponding error kernels specified by (10) are shown in the top three rows. Here, we assume the energy distribution to be a Gaussian shown in (j). The columns correspond to the interpolators with different lengths ($J = 4, 6\&8$), computed assuming $K = 68$, $N = 64$ and $O = 101$. We observe that the error kernels associated with the LS-KB scheme is much higher than the proposed one, mainly due to the sub-optimality of the scale factors as shown in Fig. 1. The decay of the NUFFT approximation error for a random k-space sampling pattern are shown in (k) and (l). We observe from (k) that the MOLS schemes provide the lowest mean-square errors. However, their worst case performance is much worse than the WOLS scheme as see from (l), since they result in higher errors at the image boundaries.

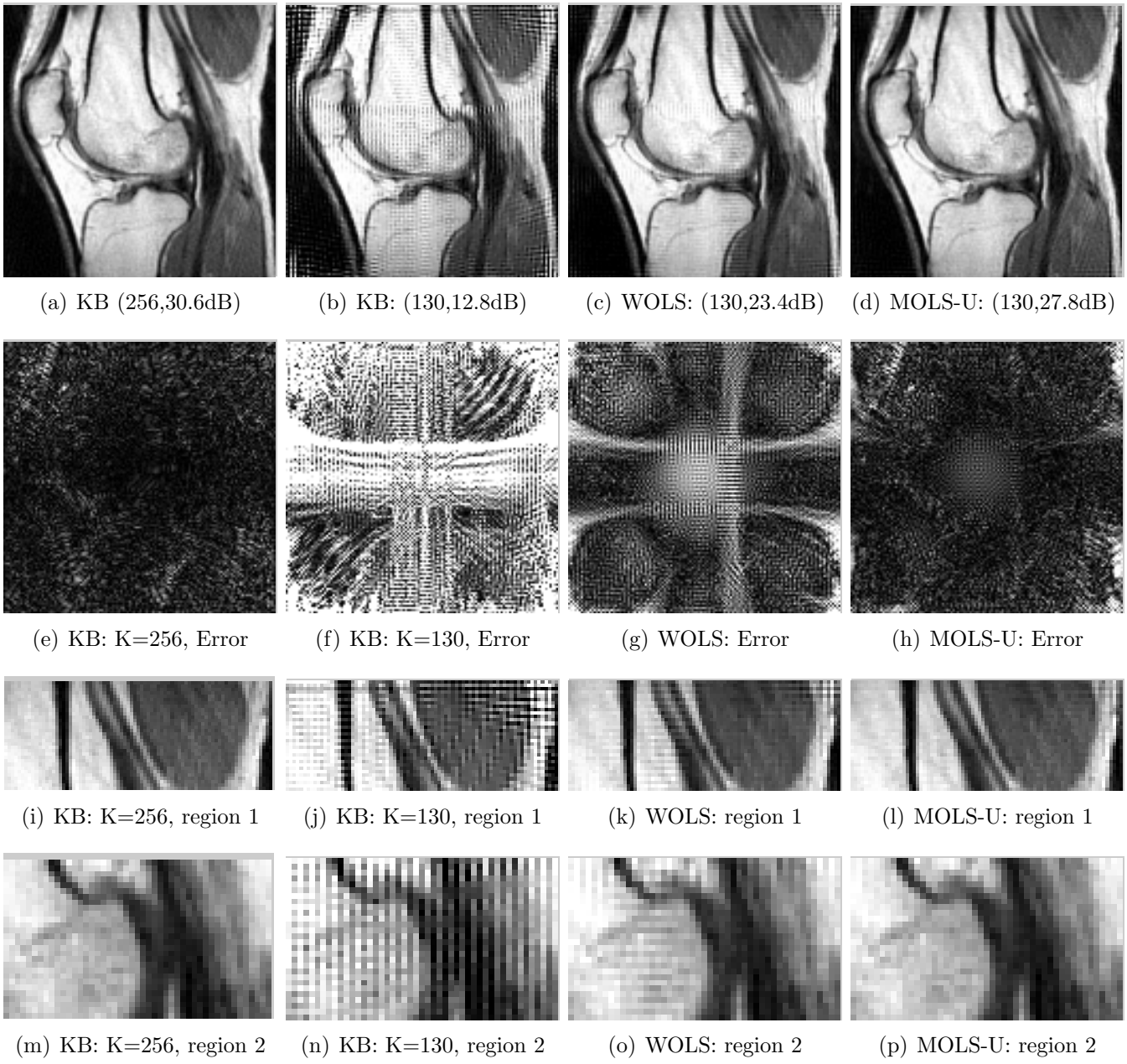

(a) KB (256,30.6dB) (b) KB: (130,12.8dB) (c) WOLS: (130,23.4dB) (d) MOLS-U: (130,27.8dB)

(e) KB: K=256, Error (f) KB: K=130, Error (g) WOLS: Error (h) MOLS-U: Error

(i) KB: K=256, region 1 (j) KB: K=130, region 1 (k) WOLS: region 1 (l) MOLS-U: region 1

(m) KB: K=256, region 2 (n) KB: K=130, region 2 (o) WOLS: region 2 (p) MOLS-U: region 2

Figure 3: Reconstructed images and error images using different interpolators on a knee MR image from 128 lines. The top row compares (a) the classical K=2N setting with KB kernel (b) Kaiser Bessel (KB) with K=130, (c) WOLS with K=130, and (d) MOLS schemes with K=130. The second row shows the reconstruction errors. The error images are scaled by a factor of 10 for better visualization. We observe that the KB reconstruction suffers from extensive artifacts, while some artifacts are visible in WOLS reconstructions. The artifacts can be better visualized in the zoomed regions of the reconstructions in the top and middle image regions, shown in third and fourth rows, respectively.

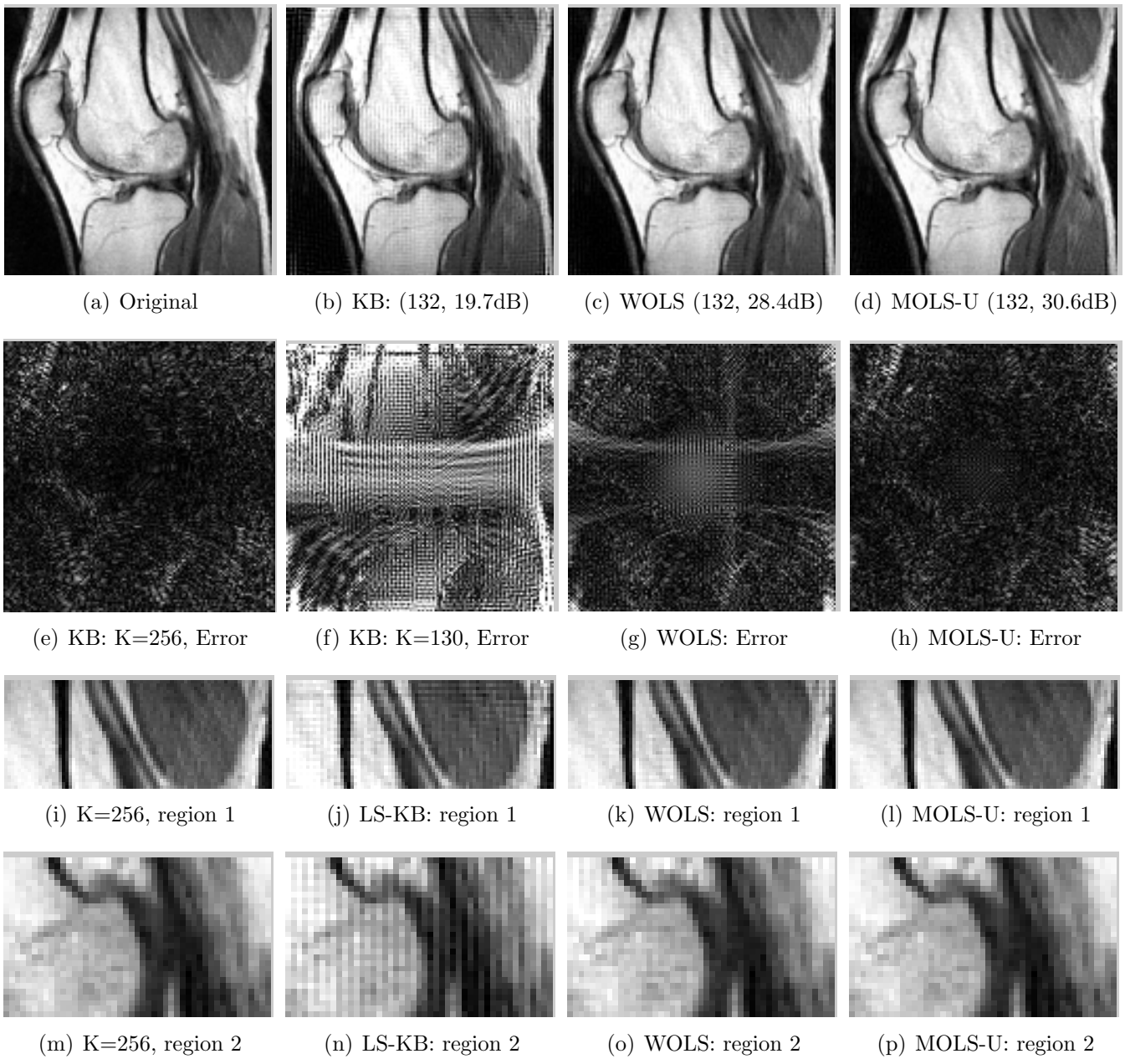

(a) Original (b) KB: (132, 19.7dB) (c) WOLS (132, 28.4dB) (d) MOLS-U (132, 30.6dB)

(e) KB: K=256, Error (f) KB: K=130, Error (g) WOLS: Error (h) MOLS-U: Error

(i) K=256, region 1 (j) LS-KB: region 1 (k) WOLS: region 1 (l) MOLS-U: region 1

(m) K=256, region 2 (n) LS-KB: region 2 (o) WOLS: region 2 (p) MOLS-U: region 2

Figure 4: Reconstructed images and error images using different interpolators on a knee MR image sampled using a 128 spoke uniform radial trajectory. The top row compares the (b) least square Kaiser Bessel (KB), (c) WOLS, and (d) MOLS-U schemes with K=132. The original knee image is shown in (a) for comparison. The KB reconstruction with K=2N is shown in Fig. 3.a. The second row shows the reconstruction errors. The error images are scaled by a factor of 10 for better visualization. We observe that the KB reconstruction with K=132 still suffers from oscillatory artifacts, while some minor artifacts are visible in WOLS reconstructions. The artifacts can be better visualized in the zoomed regions of the reconstructions in the top and middle image regions, shown in third and fourth rows, respectively. We observe that the MOLS scheme with K=132 ((d),(h),(l), and (p)) is capable of providing reconstructions that are quite comparable to the the classical K=2N reconstructions, shown in Fig. 3.a as well as Fig. 4.(e), (i) and (m). Also note that SNR figures of MOLS at K=132 are similar to the LS-KB scheme at K=256.

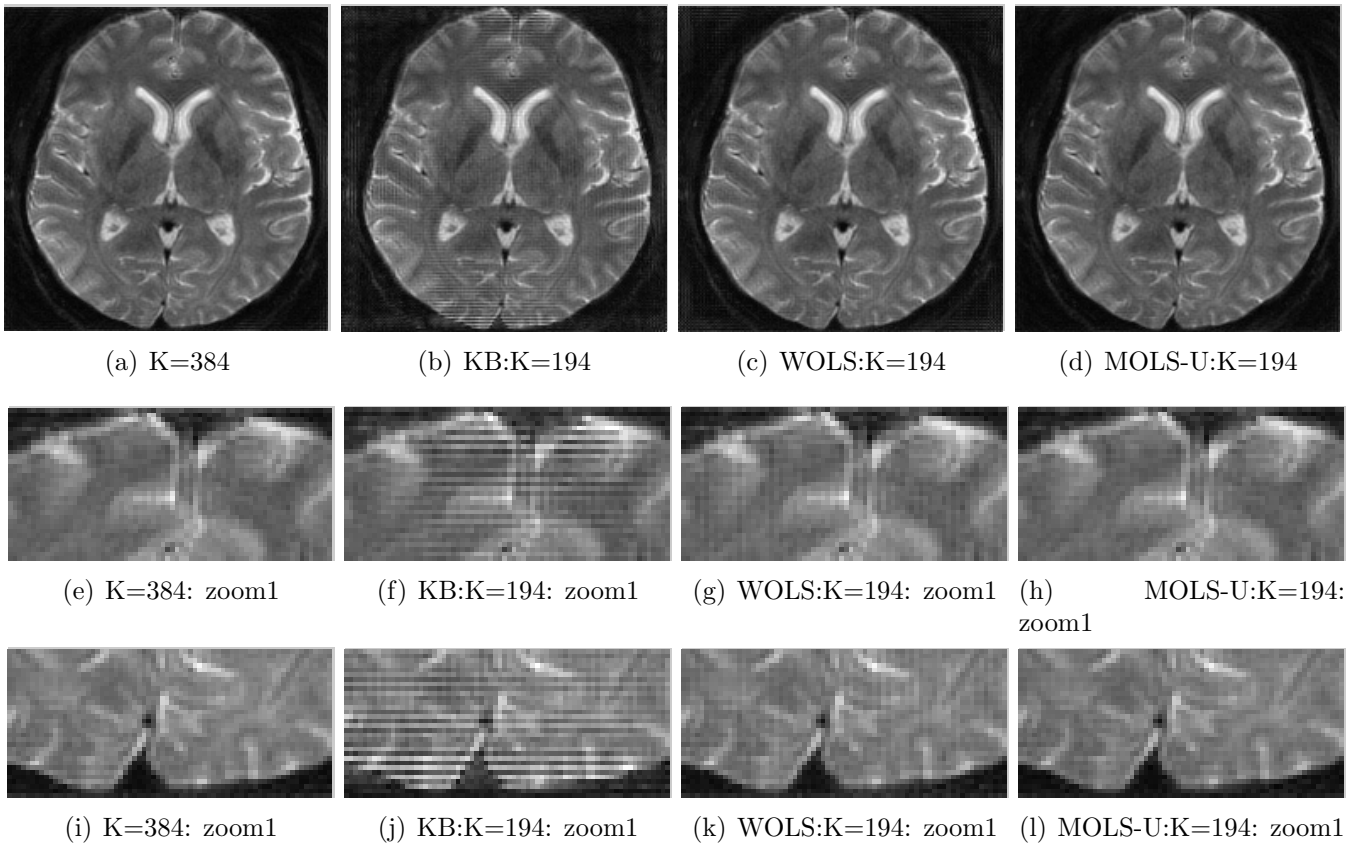

(a) K=384 (b) KB:K=194 (c) WOLS:K=194 (d) MOLS-U:K=194

(e) K=384: zoom1 (f) KB:K=194: zoom1 (g) WOLS:K=194: zoom1 (h) MOLS-U:K=194: zoom1

(i) K=384: zoom1 (j) KB:K=194: zoom1 (k) WOLS:K=194: zoom1 (l) MOLS-U:K=194: zoom1

Figure 5: Reconstructed images and error images using different interpolators on a 192x192 brain MR image from multi-channel spiral samples. The top row compares (a) the classical KB NUFFT with $K = 2N$, (b) the Kaiser Bessel (KB) scheme with K=194, (c) WOLS method with K=194, and (d) MOLS-U NUFFT with K=194. The second row and third rows correspond to zoomed image regions in the top and bottom regions, respectively. We observe that the KB reconstruction suffers from extensive artifacts, while some artifacts are visible in WOLS reconstructions. By contrast, the MOLS scheme with K=194 is capable of providing reconstructions that are quite comparable to the the classical K=2N reconstructions.